Multi-level surface enhanced Raman scattering using AgO_x thin film

Ming Lun Tseng,[1,2] Chia Min Chang,[3] Bo Han Cheng,[4] Pin Chieh Wu,[1,2] Kuang Sheng Chung,[2] Min-Kai Hsiao,[5] Hsin Wei Huang,[1,2] Ding-Wei Huang,[3] Hai-Pang Chiang,[5,7] Pui Tak Leung,[6] and Din Ping Tsai[1,2,4,*]

[1]Graduate Institute of Applied Physics, National Taiwan University, Taipei 106, Taiwan
[2]Department of Physics, National Taiwan University, Taipei 106, Taiwan
[3]Graduate Institute of Photonics and Optoelectronics, National Taiwan University, Taipei 106, Taiwan
[4]Research Center for Applied Sciences, Academia Sinica, Taipei 115, Taiwan
[5]Institute of Optoelectronic Sciences, National Taiwan Ocean University, Keelung 202, Taiwan
[6]Department of Physics, Portland State University, Portland, OR 97207 USA
[7]hpchiang@mail.ntou.edu.tw
[*]dptsai@phys.ntu.edu.tw

Abstract: Ag nanostructures with surface-enhanced Raman scattering (SERS) activities have been fabricated by applying laser-direct writing (LDW) technique on silver oxide (AgO_x) thin films. By controlling the laser powers, multi-level Raman imaging of organic molecules adsorbed on the nanostructures has been observed. This phenomenon is further investigated by atomic-force microscopy and electromagnetic calculation. The SERS-active nanostructure is also fabricated on transparent and flexible substrate to demonstrate our promising strategy for the development of novel and low-cost sensing chip.

OCIS codes: (250.5403) Plasmonics; (240.6695) Surface-enhanced Raman scattering; (310.3840) Materials and process characterization; (220.4241) Nanostructure fabrication; (140.3390) Laser materials processing.

References

1. D. P. Tsai, J. Kovacs, Z. H. Wang, M. Moskovits, V. M. Shalaev, J. S. Suh, and R. Botet, "Photon scanning tunneling microscopy images of optical excitations of fractal metal colloid clusters," Phys. Rev. Lett. **72**(26), 4149–4152 (1994).
2. C. E. Talley, J. B. Jackson, C. Oubre, N. K. Grady, C. W. Hollars, S. M. Lane, T. R. Huser, P. Nordlander, and N. J. Halas, "Surface-enhanced raman scattering from individual au nanoparticles and nanoparticle dimer substrates," Nano Lett. **5**(8), 1569–1574 (2005).
3. M. Moskovits, "Surface-enhanced spectroscopy," Rev. Mod. Phys. **57**(3), 783–826 (1985).
4. A. Barhoumi, D. Zhang, F. Tam, and N. J. Halas, "Surface-enhanced Raman spectroscopy of DNA," J. Am. Chem. Soc. **130**(16), 5523–5529 (2008).
5. X. Qian, X.-H. Peng, D. O. Ansari, Q. Yin-Goen, G. Z. Chen, D. M. Shin, L. Yang, A. N. Young, M. D. Wang, and S. Nie, "In vivo tumor targeting and spectroscopic detection with surface-enhanced raman nanoparticle tags," Nat. Biotechnol. **26**(1), 83–90 (2008).
6. A. Chou, E. Jaatinen, R. Buividas, G. Seniutinas, S. Juodkazis, E. L. Izake, and P. M. Fredericks, "SERS substrate for detection of explosives," Nanoscale **4**(23), 7419–7424 (2012).
7. W.-C. Lin, H.-C. Jen, C.-L. Chen, D.-F. Hwang, R. Chang, J.-S. Hwang, and H.-P. Chiang, "SERS study of tetrodotoxin (TTX) by using silver nanoparticle arrays," Plasmonics **4**(2), 187–192 (2009).
8. K. K. Strelau, T. Schüler, R. Möller, W. Fritzsche, and J. Popp, "Novel bottom-up SERS substrates for quantitative and parallelized analytics," ChemPhysChem **11**(2), 394–398 (2010).
9. C. L. Haynes and R. P. Van Duyne, "Nanosphere lithography: A versatile nanofabrication tool for studies of size-dependent nanoparticle optics," J. Phys. Chem. B **105**(24), 5599–5611 (2001).
10. H.-L. Huang, C. F. Chou, S. H. Shiao, Y.-C. Liu, J.-J. Huang, S. U. Jen, and H.-P. Chiang, "Surface plasmon-enhanced photoluminescence of DCJTB by using silver nanoparticle arrays," Opt. Express **21**(S5), A901–A908 (2013).
11. J. Neddersen, G. Chumanov, and T. M. Cotton, "Laser-ablation of metals - a new method for preparing SERS active colloids," Appl. Spectrosc. **47**(12), 1959–1964 (1993).
12. X. Ling, L. Xie, Y. Fang, H. Xu, H. Zhang, J. Kong, M. S. Dresselhaus, J. Zhang, and Z. Liu, "Can graphene be used as a substrate for Raman enhancement?" Nano Lett. **10**(2), 553–561 (2010).

#193820 - $15.00 USD Received 24 Jul 2013; revised 16 Sep 2013; accepted 24 Sep 2013; published 7 Oct 2013

13. T. C. Chong, M. H. Hong, and L. P. Shi, "Laser precision engineering: From microfabrication to nanoprocessing," Laser Photonics Rev. **4**(1), 123–143 (2010).
14. M. Malinauskas, P. Danilevičius, and S. Juodkazis, "Three-dimensional micro-/nano-structuring via direct write polymerization with picosecond laser pulses," Opt. Express **19**(6), 5602–5610 (2011).
15. N. R. Han, Z. C. Chen, C. S. Lim, B. Ng, and M. H. Hong, "Broadband multi-layer terahertz metamaterials fabrication and characterization on flexible substrates," Opt. Express **19**(8), 6990–6998 (2011).
16. K. Masui, S. Shoji, K. Asaba, T. C. Rodgers, F. Jin, X. M. Duan, and S. Kawata, "Laser fabrication of Au nanorod aggregates microstructures assisted by two-photon polymerization," Opt. Express **19**(23), 22786–22796 (2011).
17. C.-H. Lin, L. Jiang, Y.-H. Chai, H. Xiao, S.-J. Chen, and H.-L. Tsai, "One-step fabrication of nanostructures by femtosecond laser for surface-enhanced raman scattering," Opt. Express **17**(24), 21581–21589 (2009).
18. A. Takami, H. Kurita, and S. Koda, "Laser-induced size reduction of noble metal particles," J. Phys. Chem. B **103**(8), 1226–1232 (1999).
19. M. L. Tseng, Y.-W. Huang, M.-K. Hsiao, H. W. Huang, H. M. Chen, Y. L. Chen, C. H. Chu, N.-N. Chu, Y. J. He, C. M. Chang, W. C. Lin, D.-W. Huang, H.-P. Chiang, R.-S. Liu, G. Sun, and D. P. Tsai, "Fast fabrication of a Ag nanostructure substrate using the femtosecond laser for broad-band and tunable plasmonic enhancement," ACS Nano **6**(6), 5190–5197 (2012).
20. W. Zhu, D. Wang, and K. B. Crozier, "Direct observation of beamed Raman scattering," Nano Lett. **12**(12), 6235–6243 (2012).
21. A. J. Pasquale, B. M. Reinhard, and L. Dal Negro, "Concentric necklace nanolenses for optical near-field focusing and enhancement," ACS Nano **6**(5), 4341–4348 (2012).
22. S. Ayas, H. Güner, B. Türker, O. O. Ekiz, F. Dirisaglik, A. K. Okyay, and A. Dâna, "Raman enhancement on a broadband meta-surface," ACS Nano **6**(8), 6852–6861 (2012).
23. D. He, B. Hu, Q.-F. Yao, K. Wang, and S.-H. Yu, "Large-scale synthesis of flexible free-standing SERS substrates with high sensitivity: electrospun PVA nanofibers embedded with controlled alignment of silver nanoparticles," ACS Nano **3**(12), 3993–4002 (2009).
24. W. Xu, X. Ling, J. Xiao, M. S. Dresselhaus, J. Kong, H. Xu, Z. Liu, and J. Zhang, "Surface enhanced Raman spectroscopy on a flat graphene surface," Proc. Natl. Acad. Sci. U.S.A. **109**(24), 9281–9286 (2012).
25. A. J. Chung, Y. S. Huh, and D. Erickson, "Large area flexible SERS active substrates using engineered nanostructures," Nanoscale **3**(7), 2903–2908 (2011).
26. X. Liu, C. Zong, K. Ai, W. He, and L. Lu, "Engineering natural materials as surface-enhanced raman spectroscopy substrates for in situ molecular sensing," ACS Appl. Mater. Interfaces **4**(12), 6599–6608 (2012).
27. Y. Nagai, T. Yamaguchi, and K. Kajikawa, "Angular-resolved polarized surface enhanced raman spectroscopy," J. Phys. Chem. C **116**(17), 9716–9723 (2012).
28. A. Kocabas, G. Ertas, S. S. Senlik, and A. Aydinli, "Plasmonic band gap structures for surface-enhanced Raman scattering," Opt. Express **16**(17), 12469–12477 (2008).
29. W.-C. Lin, S.-H. Huang, C.-L. Chen, C.-C. Chen, D. P. Tsai, and H.-P. Chiang, "Controlling SERS intensity by tuning the size and height of a silver nanoparticle array," Appl. Phys., A Mater. Sci. Process. **101**(1), 185–189 (2010).
30. P. Hildebrandt and M. Stockburger, "Surface-enhanced resonance raman-spectroscopy of rhodamine-6g adsorbed on colloidal silver," J. Phys. Chem. **88**(24), 5935–5944 (1984).
31. S. Inasawa, M. Sugiyama, and S. Koda, "Size controlled formation of gold nanoparticles using photochemical grwoth and photothermal size reduction by 308 nm laser pulses," Jpn. J. Appl. Phys. **42**(Part 1, No. 10), 6705–6712 (2003).
32. T.-C. Peng, W.-C. Lin, C.-W. Chen, D. P. Tsai, and H.-P. Chiang, "Enhanced sensitivity of surface plasmon resonance phase-interrogation biosensor by using silver nanoparticles," Plasmonics **6**(1), 29–34 (2011).
33. A. F. Oskooi, D. Roundy, M. Ibanescu, P. Bermel, J. D. Joannopoulos, and S. G. Johnson, "MEEP: A flexible free-software package for electromagnetic simulations by the fdtd method," Comput. Phys. Commun. **181**(3), 687–702 (2010).
34. A. D. Rakic, A. B. Djurisic, J. M. Elazar, and M. L. Majewski, "Optical properties of metallic films for vertical-cavity optoelectronic devices," Appl. Opt. **37**(22), 5271–5283 (1998).
35. D. V. Tsu and T. Ohta, "Mechanism of properties of noble ZnS-SiO_2 protection layer for phase change optical disk media," Jpn. J. Appl. Phys. **45**(8A), 6294–6307 (2006).
36. C. H. Chu, C. D. Shiue, H. W. Cheng, M. L. Tseng, H.-P. Chiang, M. Mansuripur, and D. P. Tsai, "Laser-induced phase transitions of $Ge_2Sb_2Te_5$ thin films used in optical and electronic data storage and in thermal lithography," Opt. Express **18**(17), 18383–18393 (2010).
37. S. K. Lin, I. C. Lin, and D. P. Tsai, "Characterization of nano recorded marks at different writing strategies on phase-change recording layer of optical disks," Opt. Express **14**(10), 4452–4458 (2006).
38. C. M. Chang, C. H. Chu, M. L. Tseng, H. P. Chiang, M. Mansuripur, and D. P. Tsai, "Local electrical characterization of laser-recorded phase-change marks on amorphous $Ge_2Sb_2Te_5$ thin films," Opt. Express **19**(10), 9492–9504 (2011).

#193820 - $15.00 USD Received 24 Jul 2013; revised 16 Sep 2013; accepted 24 Sep 2013; published 7 Oct 2013

1. Introduction

Localized surface plasmon resonance (LSPR) can induce highly intense and localized electromagnetic fields near the surfaces of metallic nanostructures under illumination [1–3]. In molecular spectroscopy, the Raman scattering cross section of molecules near these "hotspots" [2] will be dramatically enhanced, known as surface-enhanced Raman scattering (SERS) [3]. SERS is very useful for sensing and characterizing DNA molecules [4], cancer cell [5], explosives vapors [6], and food toxins [7]. These applications are very important for genetics, pathogen identification, and public security, *etc*. Therefore, many approaches for fabricating LSPR-active nanostructures and substrates have been developed [8–12]. Among the many micro- and nanofabrication techniques, laser-direct writing technique (LDW) [13–16] has been proven to be very useful in fabrication of SERS-active structures [17–19]. For example, using laser pulses to treat the metal surfaces, people can make metallic nanostructures with SERS activity on the surface [17]. Moreover, recent experiments have shown that the LSPR-active Ag nanostructures can be locally fabricated on the laser-treated silver AgO_x thin film with the laser-induced chemical reduction of the AgO_x material [19], leaving the unprocessed AgO_x thin film acted as dielectric and an optically transparent background. This property makes laser-treated AgO_x thin film very promising in the integration of SERS nanostructures with various optical components [20–22]. In comparison with other LDW-based methods for SERS-active nanostructures, using AgO_x thin film can make the SERS-active layer thinner. People can also make SERS-active nanostructures into specific pattern by controlling the laser raster path. In our previous work, the SERS capability of the laser-treated AgO_x thin film is found to be varied with the processing laser power [19]. However, the origin of this experimental result is not well understood. In this paper, fabrication of Ag nanostructures from AgO_x thin film with different plasmonic enhancements is carried out with different laser powers. SERS from different Ag nanostructures is investigated using Raman spectroscopy to probe the Raman vibration signals of organic molecules located on the structures' surface. Atomic force microscopy (AFM) and electromagnetic simulation are employed to understand the relation between the Ag nanostructure morphologies and the corresponding SERS efficiencies. Moreover, many novel SERS sensors are needed to be fabricated on the flexible substrate for sensing applications on curved samples [23–26], such as human bodies and foods. The Ag nanostructure is fabricated on the transparent and flexible polycarbonate substrate for demonstrating the potential of our proposed method.

2. Experimental

AgO_x thin films are reactively sputtered on transparent BK7 substrates (thickness = 1.5 mm) by RF-magnetron sputtering machine (Shibaura Mechatronics Corp.) in an Ar/O_2 (flow ratio = 10/25) mixed-gas atmosphere (pressure of the gas mixture = 5×10^{-1} Pa). In the fabrication of Ag nanostructures, the as-deposited AgO_x thin film is mounted on the computer-controlled three-dimensional stage (Mad City Lab. Inc.) of the fs-laser system. A Ti:Sapphire fs-laser oscillator (Coherent Inc.) emitting at 800 nm, with a repetition rate and a pulse width of 80 MHz and 140 fs, respectively, is focused by an oil-immersion objective lens (Zeiss Plan-Apochromat, 100 × , working distance = 0.17 mm, NA = 1.4) through the substrate and illuminated on the AgO_x thin film. The incident laser power is adjusted by an attenuator. Before enter the objective lens, the laser beam is expended to a diameter of 6 mm, and is made circularly polarized using a λ/4 waveplate. In this work, the applied powers on the thin film are 21 mW, 11 mW, and 7 mW, which the corresponding fluences are 18.9 mJ/cm^2, 9.9 mJ/cm^2, and 6.3 mJ/cm^2, respectively.

Characterization of the Ag nanostructures is carried out using an atomic force microscope (Asylum Research, MFP-3D) for surface morphology. For Raman spectroscopy and imaging, a WITec CRM200 scanning confocal Raman microscope with 532 nm-wavelength

#193820 - $15.00 USD Received 24 Jul 2013; revised 16 Sep 2013; accepted 24 Sep 2013; published 7 Oct 2013

semiconductor laser for excitation is employed. The excitation laser beam is focused with a 100 × objective lens (NA = 0.95) on a Nikon Plan microscope. In Raman measurement, Rhodamine 6G (R6G) is used to evaluate the SERS efficiencies of the samples. In the literature, R6G has been widely utilized for studying different SERS-active structures previously, and the Raman vibration of R6G has been studied comprehensively [8, 27–30]. Drops of 10^{-5} M R6G solution are put on the sample by a dropper, and purged by pure N_2 gas. The sample is subsequently mounted on the piezostage of the Raman system and point-by-point scanned (step size = 1μm, exposure time = 1s) under excitation, while the corresponding Raman spectrum of each point is acquired in the scanning. The laser power on the sample is kept at 0.1 mW to avoid undesired laser-induced reduction of AgO_x and sample damage.

3. Results and discussions

3.1 Relations between SERS and processing laser powers on AgO_x

Figure 1(a) is the optical reflection image of the laser-processed AgO_x thin film. Three rectangular zones on an as-deposited AgO_x thin film are treated by fs-laser beam in the form of raster scanning with various fs-laser powers. The applied powers on the thin film are 21 mW, 11 mW, and 7 mW, respectively, to write parallel lines with a separation of 1 μm (scanning rate ~33.3 μm/s). In the optical image, optical reflectance of the processed area is apparently raised in comparison with the untreated one, indicating the obviously metallic property of the processed area. No obvious difference in reflectivity is observed among the regions processed with laser powers of 21 and 11 mW, and the reflectivity at the 7-mW region being slightly smaller. Even the reflections are not seen to vary with laser powers significantly, the Raman enhancements in the three regions are rather different. Figure 1(b) is the corresponding Raman intensity map image of R6G adsorbed on the area. In Raman intensity map, the regions displayed in brighter color are with higher intensity of selected Raman peak. The Raman image of intensity map shows the spatial distribution of Raman intensity integrated over the peak in the regime of 598-623 cm^{-1}, which is associated with the in-plane bending of the xanthene ring in the R6G molecule [30]. Four obvious levels of R6G Raman intensity can be observed in the image: Raman intensity at the 21-mW processed region is brighter than those at 11-mW and 7-mW, and the Raman intensity recorded from laser-processed regions are all stronger than the unprocessed one.

Figure 1(c) shows the average Raman spectra obtained from various regions on processed AgO_x thin film. Peaks at 611, 770, 1358, 1507, and 1647 cm^{-1} corresponding to R6G Raman vibration modes can be identified at the spectra acquired from laser processing regions [30]. The average intensities of Raman vibration peak at the wave number 611 cm^{-1} acquired from regions processed with laser of 21 mW, 11 mW, 7 mW, and from unprocessed region are found to be around 15900, 12120, 600, and 340 CCD counts (arbitrary unit), respectively. In comparison with the unprocessed region, the Raman signal of R6G is enhanced more than 46-fold in the 21-mW laser-processed region. The enhancements of the other main vibrational modes of R6G at 770, 1358, 1507, and 1647 are 42-, 43-, 40-, 39-fold, respectively. The Raman intensities of R6G molecules are increased with increasing processing powers, indicating that SERS capability of processed AgO_x thin film depends significantly on the incident laser power.

#193820 - $15.00 USD Received 24 Jul 2013; revised 16 Sep 2013; accepted 24 Sep 2013; published 7 Oct 2013

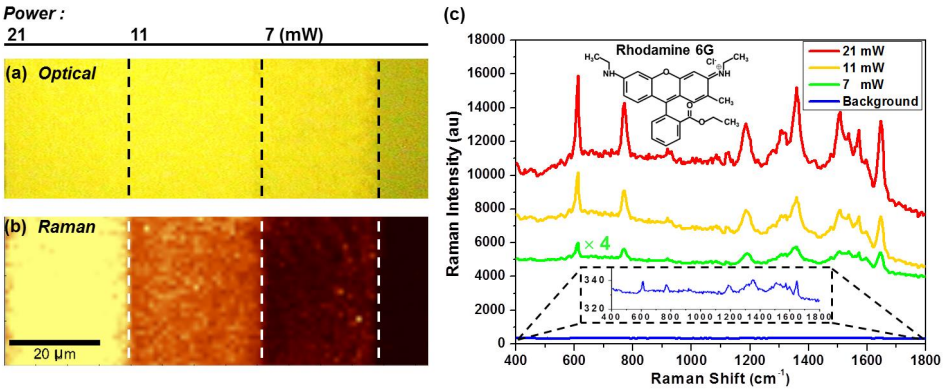

Fig. 1. (a) Optical reflection image of laser-generated Ag nanostructures made with laser powers 21 mW, 11 mW, 7 mW, respectively and (b) the corresponding Raman intensity map of R6G on the Ag nanostructures. The Raman intensity map is obtained from integrating spectral intensity of the R6G Raman peak ranging from 598 to 623 cm^{-1}. The two images are shown on the same scale. (c) Raman spectra of R6G adsorbed on various zones of laser-processed AgO_x thin film. The up insert shows the molecular structure of R6G molecule, and the button insert is the magnified Raman spectrum of R6G molecules obtained from the region of unprocessed AgO_x thin film.

Figures 2(a)-2(f) are the two-dimensional (2D-) and corresponding three-dimensional (3D) AFM images of laser-fabricated Ag nanostructures with laser power of 21 mW, 11 mW, and 7 mW, respectively. The maximum of the height scale is set as 30 nm which can get a better contrast in nanoparticle distribution in 2D-AFM images. On the other hand, for observing the evolution of height of the nanoparticles in the 3D-AFM images, the maximum of the height scale is set as 120 nm. Interestingly, the Ag nanoparticles generated with 21-mW fs-laser beam are obviously smaller than the ones generated with 7-mW fs-laser beam. This result is similar to the ones reported by Sugiyama *et al.* [31], from which the sizes of the laser-generated Au NPs (generated in $AuCl_4^-$ aqueous solution with laser-induced chemical reduction) decrease with the rise of laser power. The size reduction of the generated metallic nanoparticles can be explained by the laser-induced ablation and re-shaping in the processing [31]. The size distributions of the Ag nanoparticles shown in Figs. 2(a)-2(c) are analyzed by using *Image J* software. This image analysis method has been reported in our previous works [32]. By counting the particle number of each size, the relation between laser power and particle diameter becomes much clearer (Figs. 2(g)-2(i)). When irradiating the sample with higher laser power at 21 mW, the particle size distributed like Poisson distribution and the average particle size is located at about 30 nm. The same tendency occurs as the incident power changed to 11mW; however, the average particle size shifts to 40nm, which indicates the energy provided by laser would affect the occurrences of small particles. When the laser power is 7 mW, the average particle size is 50 nm, which is largest among these three irradiating laser power.

#193820 - $15.00 USD Received 24 Jul 2013; revised 16 Sep 2013; accepted 24 Sep 2013; published 7 Oct 2013

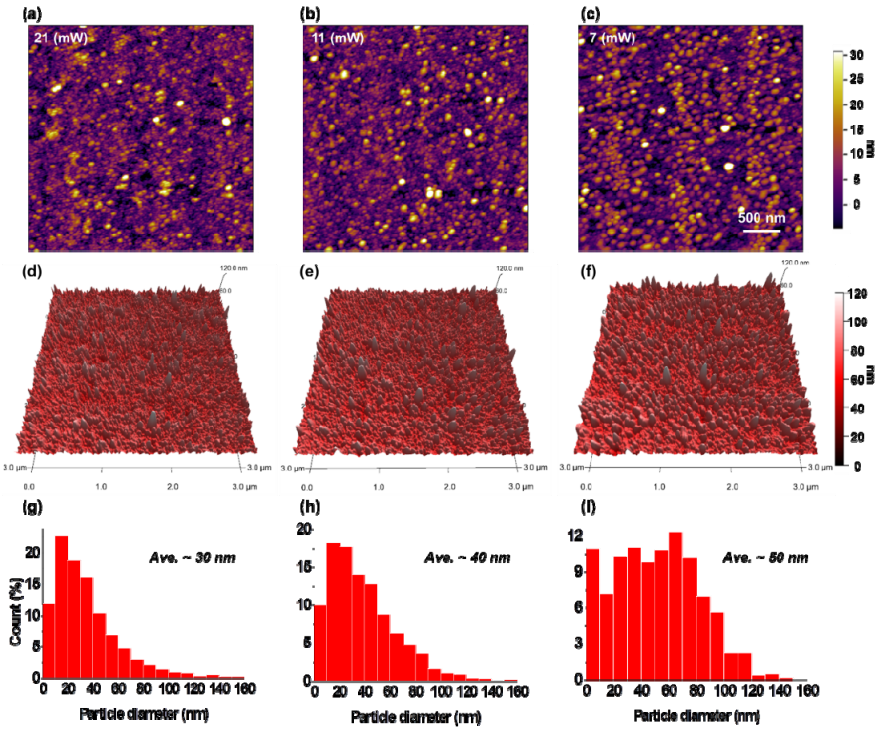

Fig. 2. (a)-(c) 2D AFM images of laser-generated Ag nanostructures with processing laser powers 21 mW, 11 mW, and 7 mW, respectively. The three images are shown on the same scale. (d)-(f) are the corresponding 3D AFM images, and (g)-(i) are the corresponding histograms of Ag NP diameters generated with various laser powers. The height scales in the 2D- and 3D- AFM images are properly adjusted for clearly demonstrating the differences of the surface morphologies between the three Ag nanostructures.

Figures 3(a) and 3(b) show the simulation electrical-field energy distribution which are obtained using MEEP (an electromagnetic simulation software package) [33]. The morphologies of Ag nanoparticles in simulation are built in accordance with the lower left corner of AFM images in Figs. 2(d) and 2(f) with the image analysis software IGOR Pro (version 6.3). The simulation region are set to be 1.1 μm × 1.1 μm × 130 nm along x, y and z direction, respectively. In the simulation process, the dimensions of grid cell are set as 1 nm in three directions, which is enough to resolve the fields at the metal-dielectric interface. All the boundary conditions in x, y and z directions are set as the perfectly matched layers that can truncate computational regions in numerical methods to simulation problems with open boundaries. The relative permittivity of Ag are given by the Lorentz-Drude model which can be expressed in the form as $\varepsilon(\omega) = 1 - \frac{\Omega_p^{\ 2}}{\omega(\omega - i\Gamma_0)} + \sum_{j=1}^{k} \frac{f_j \omega_p^{\ 2}}{(\omega_j^{\ 2} - \omega^2) + i\omega\Gamma_j}$, where ω_p is the plasma frequency, k is the number of oscillators with resonance frequency ω_j, strength f_j, and lifetime $1/\Gamma_j$ [34]. While $\Omega_p = \sqrt{f_0}\omega_p$ is the plasma frequency associated with interband transitions of oscillator strength f_0 and damping constant Γ_0. All the fitting parameters of Ag can be found in Ref [34]. The substrate material is BK7 (ε = 2.3088). According to the definition of electric-field energy $E^* \bullet D/2$, the region with positive intensity value shown in Figs. 3(a) and 3(b) indicate that the space is filled with air. Note that the areas with negative intensity indicate the region of metal. The regions with black green color (value = 0) present the internal part of the Ag nanoparticles which weakly interact with the incident wave. Comparison between the simulation results in Figs. 3(a) and 3(b) shows that more plasmon-

#193820 - $15.00 USD Received 24 Jul 2013; revised 16 Sep 2013; accepted 24 Sep 2013; published 7 Oct 2013

active sites (shown in yellow and red colors) can be observed in Fig. 3(a). On the fixed probing area, SERS of molecules adsorbed on the nanostructures will be strongly related to the area of plasmon-active sites in the laser spot. Also, since the hotspots are formed at the gaps between the nearby nanoparticles, the structure with higher surface densities of nanoparticles has more plasmon-active sites, providing stronger SERS efficiency in measurement [3].

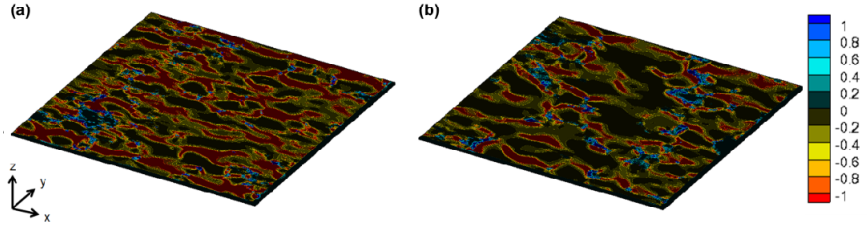

Fig. 3. Electric-filed energy slice contour ($E^* \bullet D / 2$) at the interface of Ag-BK7 under the illumination of wavelength 532 nm calculated using finite-difference time-domain (FDTD) for the laser-generated Ag nanostructures with processing laser powers (a) 21 mW and (b) 7 mW, respectively.

3.2 Fabrication of SERS surface on transparent and flexible substrate

The SERS-active Ag nanostructures can be made on the optical transparent and flexible substrate by our proposed strategy. AgO_x thin film (thickness: 15 nm) is reactively sputtered on the polycarbonate substrate (thickness = 0.6mm, refractive index~1.584). Here a 20 × Zesis Epiplan lens is utilized. For avoiding the laser-induced damage of the polycarbonate substrate, a transparent dielectric ZnS-SiO_2 film (composition ratio: ZnS 80% and SiO_2 20%) as protective layer is employed. ZnS-SiO_2 film has been widely used in the fields of optical data storage for protecting the recording media because of its high flexibility, optical transparency, low thermal conductivity, and thermal stability [35–38]. Stacked films of 200-nm-thick ZnS-SiO_2 and 15-nm-thick AgO_x are sputtered on the polycarbonate substrate. This layered structure is highly transparent and flexible. After laser processing (power: 11mW, scanning rate: 55 μm/s, spacing between scanning lines: 250 nm) Ag nanostructures are formed on the surface. As shown in Fig. 4, obvious Raman enhancement for R6G is obtained at the laser-generated Ag nanostructure on flexible substrate.

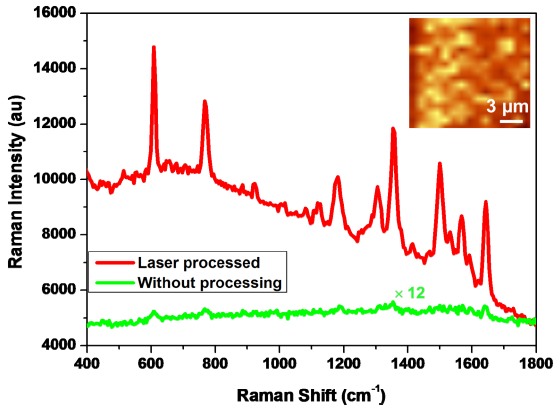

Fig. 4. Raman spectra of R6G molecules obtained from the laser-generated Ag nanostructure and as-deposited AgO_x thin film on optical transparent and flexible substrate. The Raman image of intensity map shows the spatial distribution of Raman intensity integrated over the peak in the regime of 598-623 cm^{-1}.

#193820 - $15.00 USD Received 24 Jul 2013; revised 16 Sep 2013; accepted 24 Sep 2013; published 7 Oct 2013

4. Conclusion

We have reported an efficient method to fabricate SERS-active Ag nanostructures by using laser-direct writing to treat sputtered AgO_x thin films. The multi-level Raman enhancements of R6G molecules observed in our experiments have their origins from the different average sizes of the generated Ag nanoparticles on the surfaces. These sizes can be controlled by the laser power, leading to different plasmon-active areas on the fixed probing area. In addition, proof-of-principle demonstration of making SERS-active structures on the flexible substrate is also presented. The present methodology is thus very promising for future applications of SERS to sensing and fabrication of lab-on-chip systems.

Acknowledgments

The authors gratefully acknowledge the financial support of the National Science Council of Taiwan (NSC 102-2745-M-002-005-ASP, 102-2911-I-002-505, 100-2112-M-019-003-MY3). They are also grateful to National Center for Theoretical Sciences, Taipei Office, Molecular Imaging Center of National Taiwan University, National Center for High-Performance Computing, Taiwan, and Research Center for Applied Sciences, Academia Sinica, Taiwan for their support.

#193820 - $15.00 USD Received 24 Jul 2013; revised 16 Sep 2013; accepted 24 Sep 2013; published 7 Oct 2013